Remote Sensing Image Thresholding for Landslide Motion Detection

Paul L. Rosin, Javier Hervás, José I. Barredo

***Abstract*— Techniques for performing change detection are developed and applied to digital aerial photographs of the Tessina landslide in Italy. Several automatic thresholding algorithms are compared, and a variety of filters are employed to eliminate much of the undesirable residual clutter in the thresholded difference image, mainly as a result of natural vegetation and man-made land cover changes. This has enabled us to discriminate most ground surface changes related to landslide movement.**

I. Introduction

OPTICAL (visible-infrared) remote sensing has hardly been used so far for direct landslide monitoring. A major reason for this has been the insufficient spatial resolution provided until very recently by most spaceborne earth observation systems. Efforts have thus mainly concentrated on mapping possible indirect indicators of landsliding such as land cover pattern disruption and hummocky slope surfaces (e.g. [1], [2]). In contrast, differential SAR interferometry (DINSAR) has proved capable of measuring landslide centimetric displacements [3]. However, its application is constrained by SAR imaging geometry with respect to slopes, spatial resolution and signal phase decorrelation due to both vegetation and soil moisture changes between SAR data takes. The recent availability of 1m-resolution optical imagery from the Ikonos-2 satellite opens however new prospects for landslide monitoring over extensive areas. To evaluate the potential application of these new images to detect ground surface changes as a result of major slope movements, we have developed and applied change detection and thresholding methods on existing aerial photographs over the Tessina landslide in Veneto, Italy.

The Tessina landslide has developed on Eocene flysch deposits composed of marl, sandstone and calcareous units overlaying Jurassic limestone [4]. It affects an area covered mainly by grassland and woodland with some orchards, small villages and scattered houses. The movement consists of a series of rotational slides at its head quickly transforming into a 2km-long mudflow. Surficial Quaternary deposits including colluvium and glacial till have also been mobilised by the landslide. The Tessina landslide, which was first triggered in 1960, has since undergone a number of movement episodes, some of which have disrupted communication and threatened various villages. The latest major reactivation of the landslide occurred in 1992, when its surface increased from 454,000 to 500,000 m^2 [4], [5]. The landslide has since been intensively monitored by ground-based techniques [4].

Paul L. Rosin is with the Department of Computer Science, Cardiff University, UK. Email: P.L.Rosin@cs.cf.ac.uk

Javier Hervás and José I. Barredo are with the Space Applications Institute, EC Joint Research Centre, Ispra, VA, Italy. Email: javier.hervas@jrc.it

Photographic prints of Tessina exist from a number of flights from 1954 to 1994, therefore spanning several reactivation periods. Many of them, however, could not be suitably used for image processing since either diapositives (for precise scanning) or camera calibration data were not available. It was thus decided to focus this experiment on mapping ground surface changes in the landslide body and adjacent areas as a consequence of the 1992 reactivation, for which black and white aerial photographs acquired on 28/09/88, 31/08/89 and 7/10/94 at 1:75,000 scale were available. The photograph diapositives were scanned at 14 micron to produce the 1m-resolution digital images used in this experiment.

II. Image Pre-processing

In order to apply change detection and thresholding techniques on multitemporal remotely sensed images, these must first be geometrically registered and radiometrically normalised. Geometrical registration of aerial photographs of hilly areas require orthorectification of the single frames to remove effects caused both by central projection imaging and relief displacements.

To orthorectify our images, a 20m-resolution digital elevation model (DEM) of the area was generated from an aerial photograph stereopair using digital photogrammetric techniques. For this process, the 31/08/89 photographs were used because their lower shadowing effects enable better ground feature matching on the photo stereopair. Orthorectification was first accomplished for one of the photographs of 31/08/89 with the help of the 20m DEM. Orthophotos were then produced from the 1988 and 1994 photographs using the same DEM and the 1989 orthophoto as reference for GCP collection.

The 1994 orthoimage was then radiometrically normalised to the 1988 orthoimage by applying gain and bias coefficients derived from regression analysis between the two images [6], [7]. Radiometric normalisation was required to remove pixel value differences due to varying illumination, shadowing and atmospheric conditions, as well as to different camera and film response. These two images had been selected for our change detection analysis since their dates were more similar in relation to illumination effects and vegetation phenology.

After this stage the images are differenced. This is the most widely used method for change detection, and is both simple and relatively effective compared to more sophisticated approaches [8].

III. Thresholding Techniques

Having created the difference image it is generally required to threshold it into (say) two classes to provide a "change" and "no-change" classification. Over the years many methods have been developed for image thresholding (e.g. see [9]), but few are directly applicable for change detection since they generally make assumptions that do not hold true in that context. For instance, many require the distribution of difference image intensities to be bimodal, and furthermore, the size of the modes should not differ too greatly. However, even in situations where two underlying classes exist, when one is much larger than the other, its contribution to the histogram is so great that it tends to swamp and effectively obliterate the presence of the other class, leaving a unimodal distribution. This has lead to the recent development of several thresholding algorithms designed to operate under such conditions [10]. These are briefly described below.

A. Normal and LMedS Methods

In many instances it is reasonable to assume that the image noise can be modelled by a zero mean Normal distribution $N(0, \sigma^2)$. In this case, analysing the difference in intensity images is straightforward. Differencing followed by taking the absolute value will produce the Normal distribution $2N(0, 2\sigma^2)$ for positive values only. When thresholding at $x\sigma$ the probability of incorrectly classifying a pixel as change is

$$P_F = \operatorname{erfc}\left(\frac{x}{\sqrt{2}\sigma}\right).$$

This enables us to choose a suitable threshold τ for a given acceptable proportion of false change pixels.

In practice the variance of the noise is often unknown and so it needs to be estimated from the image. This can be done from the data in the standard fashion. Alternatively, we have used the more robust Least Median of Squares (LMedS) method which is insensitive to large amounts of outliers while remaining computationally efficient.

B. Poisson Method

If we assume that the noise is white then its spatial distribution over the image will be random. For the analysis of spatial data there are many measures of randomness [11], often based on the assumption that the observations follow a Poisson distribution. Since a Poisson distribution has its mean equal to its variance then the ratio of the sample variance to the sample mean is a natural test for that distribution, and is called the *relative variance*

$$V_r = \frac{s^2}{\bar{x}}.$$

It is calculated by first counting the number of observations (in our case the number of above threshold pixels in the difference map) in n windows, $x_{i=1\ldots n}$, from which the mean, $\bar{x}$, and variance, s^2, of the x_i can be found. Although the test is sensitive to the window size and point density it works adequately as long as $\bar{x}$ is sufficiently large (e.g. $\bar{x} > 1$).

For our purposes we do not wish to detect the spatially random noise, but rather to avoid it in out thresholded image. This is achieved when there is more clustering than a Poisson distribution, and is signalled by $V_r > 1$. We therefore select the threshold which maximises the relative variance, thereby maximising "clumpiness" (regions of change) and minimising the Poisson distribution (noise).

C. Connectivity Method

The location, size, and number of the regions of change are generally unknown. However, we might expect that these properties will remain fairly stable over a wide range of threshold values. This is in contrast to regions occurring in the thresholded difference map due to noise; down at the noise level small changes in the threshold value can substantially alter the number of regions. Such an observation suggests that if a range of threshold values is found that leads to a stable number of regions, then these regions are unlikely to come from noise, and so a value from this range will provide a suitable threshold. This approach was suggested by O'Gorman [12] for intensity image thresholding. Rather than counting the number of regions the image's Euler number can be used, and was found to give almost identical results at much lower computational cost.

The shape of the histogram of Euler number/threshold is modelled as a decaying exponential, and a suitable partition point between the signal and noise is the "corner" of the curve which is detected as the point on the curve with maximum deviation from the straight line drawn between the end points of the curve.

D. Corner Method

It was found that applying the Corner Method directly to the difference image histogram, also gave good results. This has been analysed and demonstrated extensively in [13].

IV. Shape Description

There are a host of techniques available for describing the shape of regions [14]. The majority attempt to extract a descriptive property from the region such as compactness, elongatedness, and convexity. The effectiveness of these properties will depend on the reliability of their computation in the presence of noise, as well as their specificity with regard to their specific application.

Because of their omnipresence in human environments, there is also a substantial body of descriptors for standard geometric shapes such as ellipses, triangles, and rectangles [15]. We use in this work the standard method for estimating the rectangularity of a region, which is the ratio of the region's area against the area of its minimum bounding rectangle (MBR). The MBR can be efficiently calculated using Toussaint's optimal, linear algorithm [16]. Although the MBR is potentially sensitive to noise a comparison against some alternative algorithms for measuring rectangularity showed it to work relatively well [17].

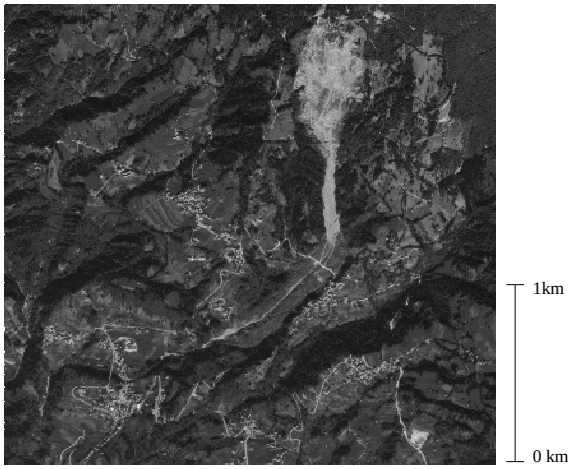

(a) 1988

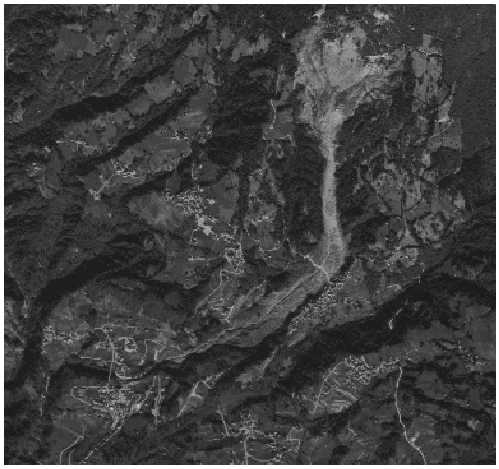

(b) 1994

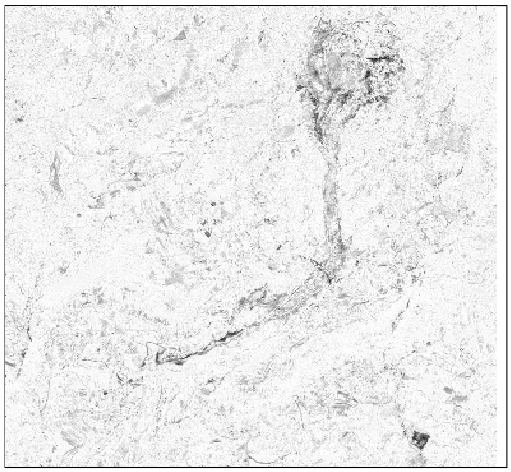

(c) difference image

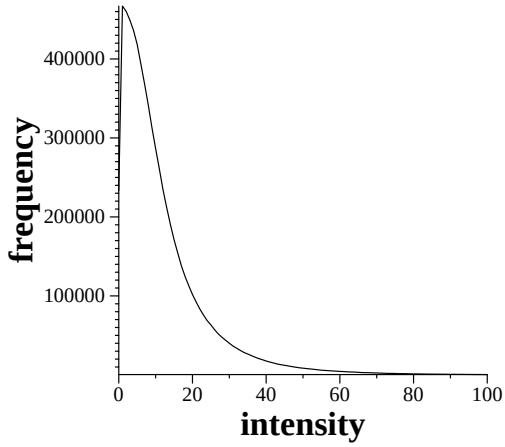

(d) difference histogram

Fig. 1. Images of Tessina before and after the landslide reactivation with the difference image

V. Experiments

Figure 1a&b shows images of the Tessina area covering the period before and after the most recent major landslide movement. The landslide runs from near the top right corner to the centre bottom left of the images; the thinner sector represents the mudflow. After some cropping their size is 2703×2590. The difference image (figure 1c; black indicates high change, white low change) is calculated by taking the absolute difference of the pixel intensity values over the two dates. Examination of the histogram of the difference image shows it to be close to a folded Normal (figure 1d). The irregularity close to zero may be an artifact of incomplete radiometric or geometric registration.

Figure 2 shows the effects of applying the thresholding methods described in section III to the difference image. In addition, three standard image thresholding methods which cover a wide range of the available techniques are applied. These are based on statistics [18], moments [19], and entropy [20]. It can be seen that there are significant similarities between some of the results, e.g. the righthand column, while the few remaining algorithms appear as outliers.

Changes detected by the corner, moments, Normal, LMedS and Poisson algorithms include on the one hand those within the landslide body surface as a result of the 1992 movement (for instance new soil outcrops because of disruption of the vegetation cover) and those produced after the movement on stable sectors of the landslide prior to the second image acquisition. These generally represent vegetation growth together with local soil moisture increase during the relative stability period following the 1992 reactivation. These findings are confirmed by interpretation of both ground photographs and low altitude aerial photographs taken during the 1992 movement period, and are in agreement with reports in [4] and [5]. The other changes detected by these five methods correspond mainly to man-made changes which include changes on grass parcels, orchards, new roads, tracks, and houses, as well as some tree canopy changes on woodland areas. Much of the noise is due to the residual effects after radiometric normalisation which are more severe in woodland areas. The statistical and especially the connectivity methods have overestimated the changes, while the entropy method has underestimated the changes.

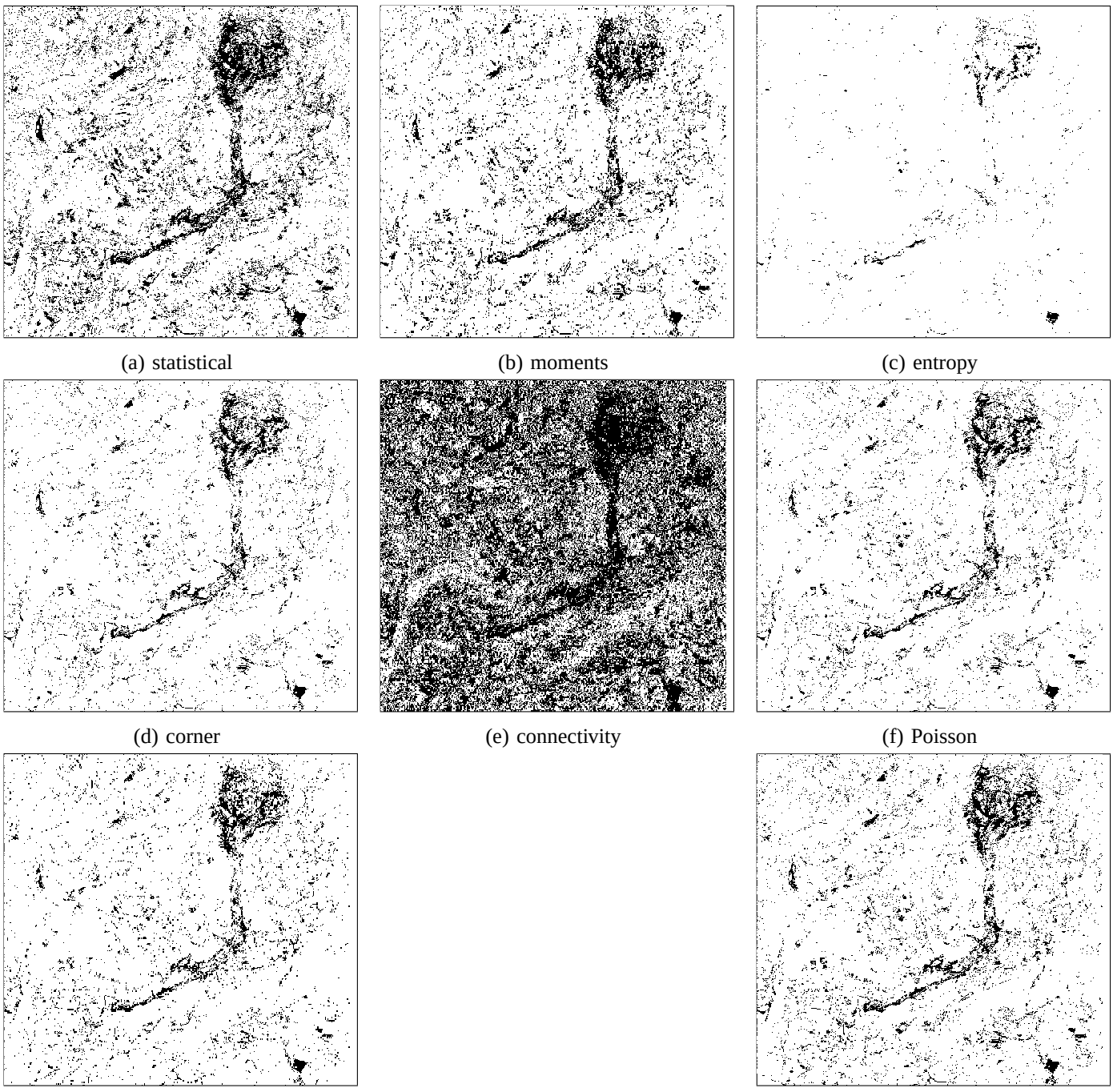

(a) statistical (b) moments (c) entropy

(d) corner (e) connectivity (f) Poisson

(g) LMedS (h) Normal

Fig. 2. Binary change map produced by thresholding the difference image

A. Blob Filtering

It is evident that simple thresholding is not sufficient to identify the true changes from the difference image. We therefore considered improving the raw thresholded output by filtering out the undesirable change blobs. This can be done based on the local properties of the blobs; we consider the following: size (area) and shape (width, perimeter and rectangularity).

In addition, more global properties also play a rôle, and we take into account the spatial relationships between blobs (density). The following sections describe the implementation of these filters and show their application to the thresholded image obtained from the corner method (see figure 2d).

B. Width and Density

To eliminate blobs according to their width the well-known erosion and dilation operators are used. Applying n iterations of erosion followed by n dilations will eliminate blobs whose width is less than $2n$. To encourage grouping of fragmented

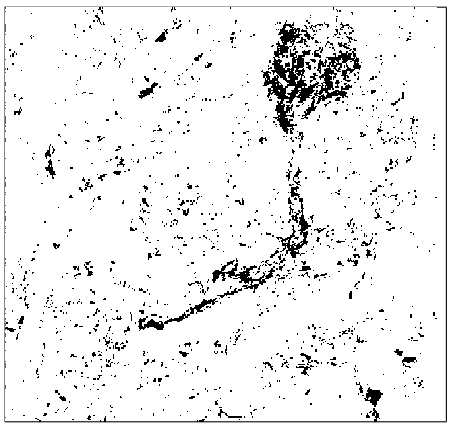

(a) erosion/dilation: 2 iterations

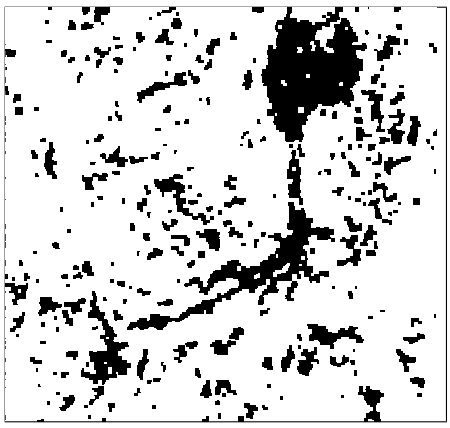

(b) erosion/dilation: 9 iterations

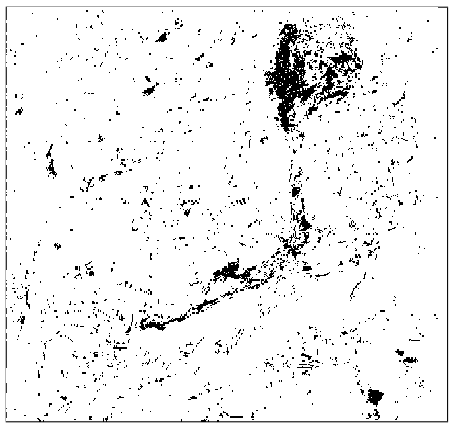

(c) perimeter > 30

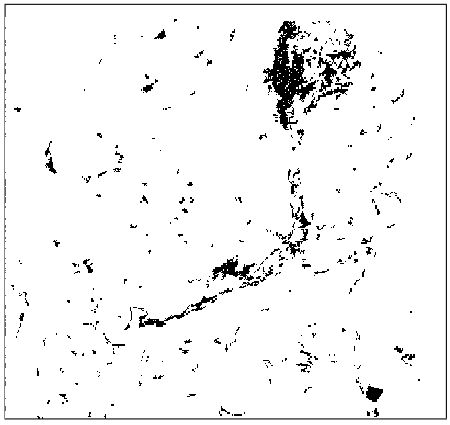

(d) perimeter > 100

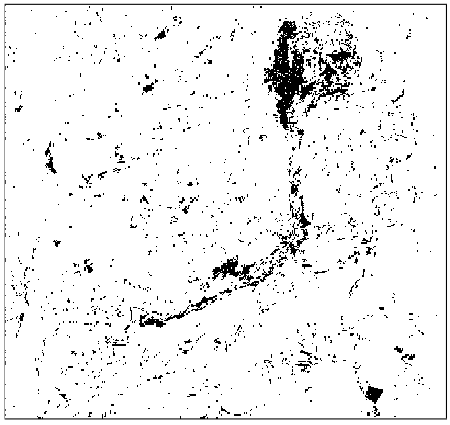

(e) area > 52

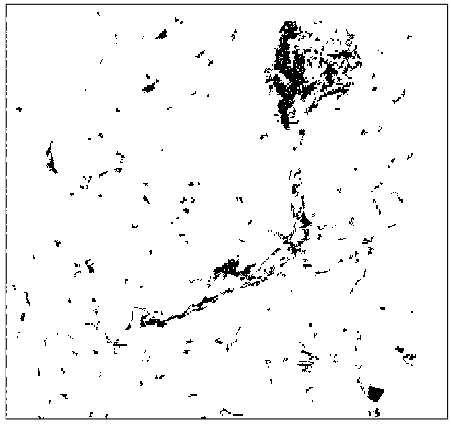

(f) area > 266

(g) erosion/dilation/area:
9 iterations & area > 1000

Fig. 3. Filtering using width, perimeter, and area

blobs, i.e. the merging of pixels in dense areas, the same process can be run in reverse. Thus the results shown in figure 3a&b are generated by the sequence of n dilations, $2n$ erosions, n dilations. From the figures it can be seen that small amounts of filtering are sufficient to remove small noise blobs as well as thin structures such as paths/roads. Higher levels of filtering successfully connect the fragmented blobs within the landslide body to form a few unified regions of change. The drawback is that the man-made and vegetation changes away from the landslide are amplified.

C. Perimeter

Calculating the perimeter of the blobs requires the blobs to be isolated (unlike the previous filter step) which is carried out using connected component labelling. (Unfortunately the boundaries of objects and holes that we obtain are not distinguished, and so this causes some minor artifacts in the processing.) The perimeter filter was applied to figure 2d with two

perimeter thresholds set to produce similar numbers of blobs as the width filtering. Figure 3c&d shows that narrow man-made features like new roads and tracks are better retained compared to width filtering, although for this application that is actually a disadvantage. At higher levels of filtering most of the landslide-related changes are retained while removing much of the extraneous changes.

D. Area

Having isolated the blobs their area can be easily calculated, and again appropriate thresholds are set to keep similar numbers of blobs as before. It can be seen from figure 3e&f that both the area and perimeter methods produce very similar results. Most of the changes outside the landslide have been removed and the major regions of change have been discriminated although their boundaries are coarsely delineated. Nevertheless, overall width filtering was more successful. Of course, combinations of filters can be applied in order to capitalise on their individual merits. Although the high level of width filtering in figure 3a created undesirable large noise blobs these can be removed by an area filter as shown in figure 3g, in which the true regions of change within the landslide have been fairly well discriminated, although the overall boundaries have been very coarsely delineated.

E. Rectangularity

Many of the man-made changes have simple polygonal shapes such as rectangular buildings, agricultural fields, and even some road segments. In some cases it would be useful to apply filtering to identify these objects. In this case however, we just wish to eliminate them since they do not typically correspond to effects of the landslide. The effects of rejecting and retaining blobs according to their measured rectangularity in combination with perimeter and area filtering are shown in figure 4. A suitable rectangularity threshold was selected by analysing the graph of the number of blobs retained after filtering against the threshold value, see figure 5. The rectangularity of most blobs is near the middle of the range. Since only a relatively small number of highly rectangular blobs are expected the upper bend at high rectangularity values is a suitable threshold as this occurs at the point just above the rectangularity values of the majority of the change blobs. The corner finding approach previously described for threshold selection was applied, and produced the value 0.6 which is used for all these examples. In all cases rectangularity has successfully identified most man-made changes.

When low levels of perimeter and area filtering were applied it appears that many small regions are classified as being highly rectangular. This can be explained by the fact that image discretisation imposes a restriction on the range of possible shapes at that scale, and the rectilinear grid often results in small blobs appearing rectangle like.

VI. Conclusions and Future Work

The application of thresholding methods to difference images derived from digital aerial photographs has proved useful to map ground surface changes related to landslide motion. The processing sequence finally adopted consisted of (1) orthorectifying and radiometrically normalising the raw images to generate images which are both geometrically and radiometrically comparable; (2) differencing the preprocessed images; (3) preliminary thresholding the difference image using the histogram corner method; (4) rectangularity-filtering the thresholded image in combination with area filtering to remove most man-made change blobs. Alternatively, perimeter filtering could be used instead of area filtering with similar effects.

Some constraints to this method were however found that are mainly due to the single-band wide spectral range of aerial photographs, lack of image calibration, and especially to possible man-made and natural changes occurring during the long time elapsed between the available photos. The latter, in particular, may mask actual movement in some landslide sectors. This can however be partly overcome by making assumptions based on image analysis and field checking.

Because of the repetitive observations starting to be provided by high spatial resolution satellites with multispectral imaging capabilities, the methods reported in this paper could become complementary to ground-based techniques for landslide monitoring on extensive areas at scales up to 1:10,000.

Figure 6 illustrates that splitting up positive and negative change to further discriminate changes associated with landslide reactivation is part of our current research. For instance, white within the landslide body indicates ground change patterns mostly associated with the reactivation occurred in 1992 whereas pixels in black appear mostly associated with either simple land cover changes or soil moisture increase. A major research effort, however, will still be needed to derive landslide movement rates from optical satellite imagery. To this end we are investigating several promising alternative approaches like the application of Anandan's [21] optical flow techniques (figure 7).

Acknowedgements

This work has been partly funded by the European Commission, DG Research, Framework Programme IV, Environment and Climate Programme, Natural Risks (A. Ghazi, head of unit; M. Yeroyanni, scientific officer) within the RUNOUT project. Thanks are also due to F. Mantovani, of University of Ferrara, Italy, and A. Pasuto and S. Silvano, of IRPI-CNR, Padua, Italy, for providing ground truth.

References

[1] J. Hervás, P.L. Rosin, A. Fernández-Renau, J.A. Gómez, and C. León, "Use of airborne multispectral imagery for mapping landslides in Los Vélez district, south-eastern Spain," in *Landslides*, J. Chacón, C. Irigaray, and T. Fernández, Eds., pp. 353–361. Balkema, 1996.

[2] P.J. Mason, M. Rosenbaum, and J.McM. Moore, "Digital image texture analysis for landslide mapping," in *Geohazards in Engineering Geology*, J.G. Maund and M. Eddleston, Eds., vol. 15, pp. 297–305. Geological Society, Engineering Geology Special Publications, 1998.

[3] H. Rott, B. Scheuchl, A. Siegel, and B. Grasemann, "Monitoring very slow slope movements by means of SAR interferometry: A case study from a mass waste above a reservoir in the Otzal Alps, Austria," *Geophysics Research Letters*, vol. 26, pp. 1629–1632, 1999.

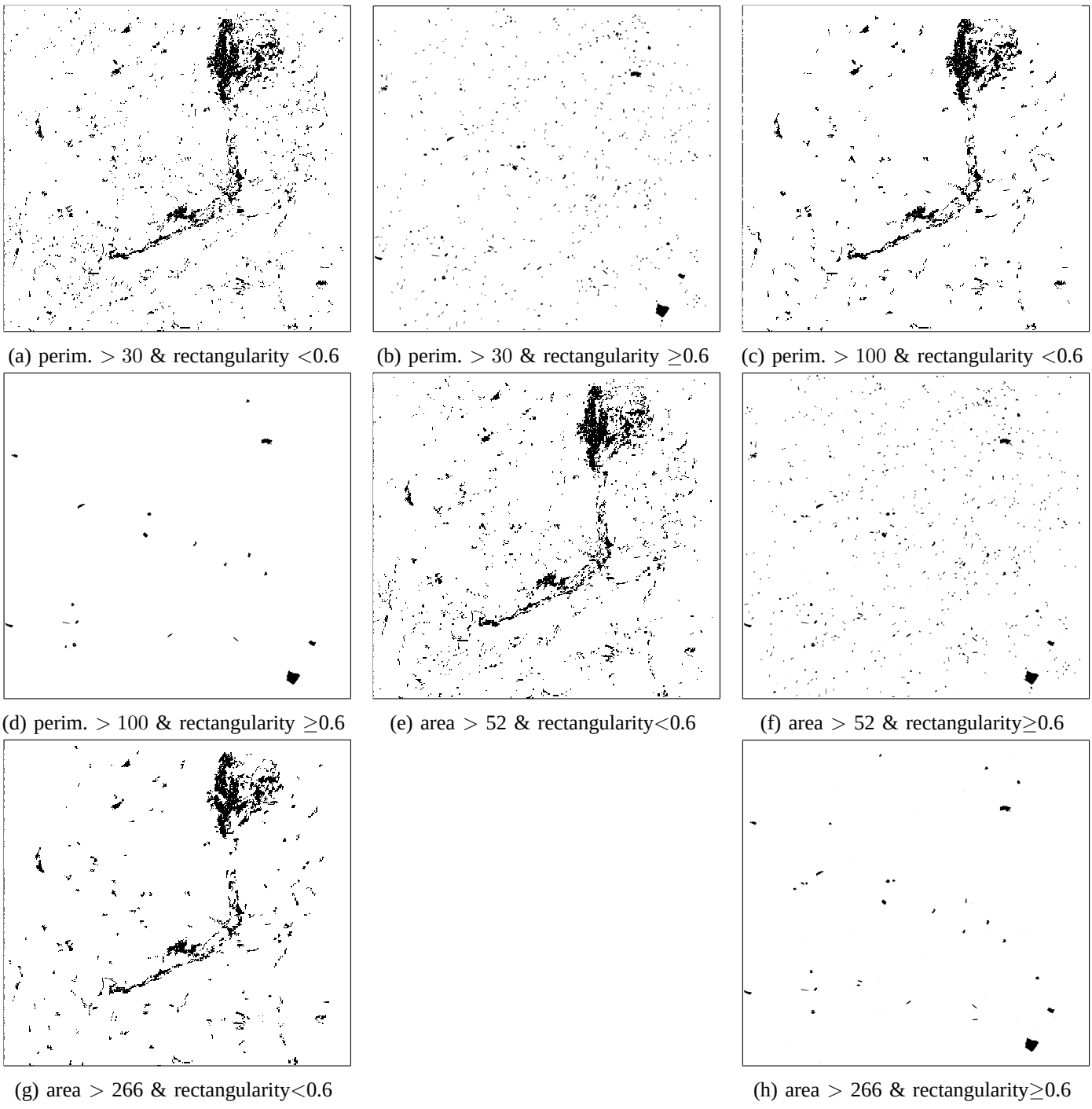

(a) perim. >30 & rectangularity <0.6 (b) perim. >30 & rectangularity ≥ 0.6 (c) perim. >100 & rectangularity <0.6

(d) perim. >100 & rectangularity ≥ 0.6 (e) area >52 & rectangularity<0.6 (f) area >52 & rectangularity≥ 0.6

(g) area >266 & rectangularity<0.6 (h) area >266 & rectangularity≥ 0.6

Fig. 4. Additionally filtering blobs using rectangularity

[4] A. Pasuto, S. Silvano, and G.P. Bozzo, "The Tessina landslide (Belluno, Italy)," in *First European Intensive Course on Applied Geomorphology*, M. Panizza, M. Soldati, and D. Barani, Eds., pp. 63–69. Istituto di Geologia, Universtità degli Studi di Modena, Italy, 1993.

[5] M.C. Turrini, N. Abu-Zeid, E. Semenza, P. Semenza, and A. El-Naqa, "New studies on the Tessina landslide," in *7th International IAEG Congress*, pp. 1667–1675. 1994.

[6] F.G. Hall, D.E. Strebel, E. Nickenson, and S.J. Goetz, "Radiometric rectification: toward a common radiometric response among multidate multisensor images," *Remote Sensing of Environment*, vol. 35, pp. 11–27, 1991.

[7] J. Hill and B Sturm, "Radiometric correction of multitemporal Thematic Mapper data for use in agricultural land-cover classification and vegetation monitoring," *Int. J. Remote Sensing*, vol. 12, pp. 1471–1491, 1991.

[8] A. Singh, "Digital change detection techniques using remotely sensed data," *Int. J. Remote Sensing*, pp. 989–1003, 1989.

[9] P.K. Sahoo, S. Soltani, A.K.C. Wong, and Y.C. Chen, "A survey of thresholding techniques," *Computer Vision, Graphics and Image Processing*, vol. 41, pp. 233–260, 1988.

[10] P.L. Rosin, "Thresholding for change detection," *Computer Vision and Image Understanding*, vol. 86, no. 2, pp. 79–95, 2002.

[11] G.J.G. Upton and B. Fingleton, *Spatial Data Analysis by Example, Volume 1, Point Pattern and Quantitative Data*, Wiley, 1985.

[12] L. O'Gorman, "Binarization and multithresholding of document images using connectivity," *CVGIP: Graphical Models and Image Processing*,

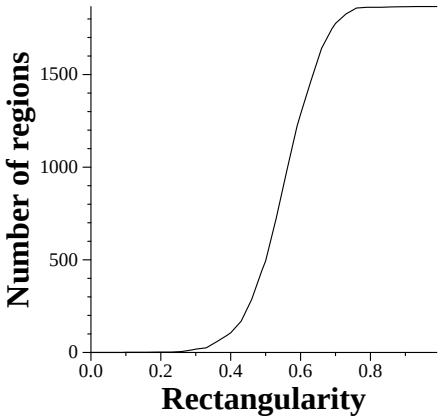

Fig. 5. Number of blobs vs rectangularity threshold

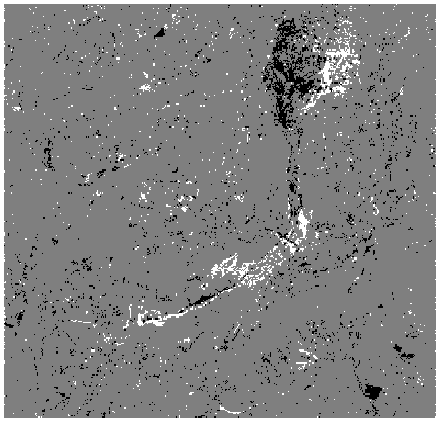

Fig. 6. Differentiating between positive and negative intensity changes

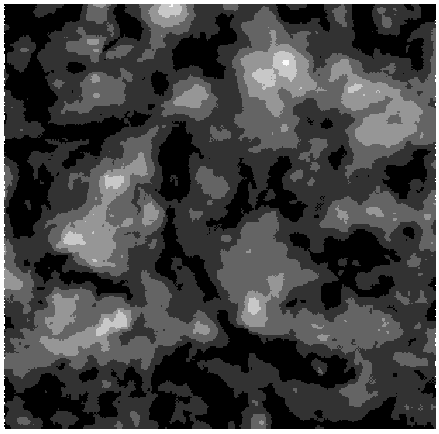

Fig. 7. Optical flow over the image pair

vol. 56, no. 6, pp. 494–506, 1994.

[13] P.L. Rosin, "Unimodal thresholding," in *Scand. Conf. Image Analysis*, 1999, pp. 585–592.

[14] M. Sonka, V. Hlavac, and R. Boyle, *Image Processing, Analysis, and Machine Vision*, Chapman and Hall, 1998.

[15] P.L. Rosin, "Measuring shape: Ellipticity, rectangularity, and triangularity," in *Int. Conf. Pattern Recognition*, 2000.

[16] G.T. Toussaint, "Solving geometric problems with the rotating calipers," in *IEEE MELECON '83*, 1983, pp. A10.02/1–4.

[17] P.L. Rosin, "Measuring rectangularity," *Machine Vision and Applications*, vol. 11, pp. 191–196, 1999.

[18] N. Otsu, "A threshold selection method from gray-level histograms," *IEEE Transactions on Systems, Man and Cybernetics*, vol. 9, pp. 62–66, 1979.

[19] W.H. Tsai, "Moment-preserving thresholding," *Computer Vision, Graphics and Image Processing*, vol. 29, pp. 377–393, 1985.

[20] J.N. Kapur, P.K. Sahoo, and A.K.C. Wong, "A new method for gray-level picture thresholding using the entropy of the histogram," *Computer Vision, Graphics and Image Processing*, vol. 29, no. 3, pp. 273–285, 1985.

[21] P. Anandan, "A computational framework and an algorithm for the measurement of visual motion," *International Journal of Computer Vision*, vol. 2, no. 3, pp. 283–310, 1989.